ACS Catalysis

Research Article

pubs.acs.org/acscatalysis

Active Coordinatively Unsaturated Manganese Monoxide-Containing Mesoporous Carbon Catalyst in Wet Peroxide Oxidation

Lina Kong,[†] Wei Wei,[†] Qingfei Zhao,[†] Jian-Qiang Wang,[‡] and Ying Wan*[,†]

[†]Key Laboratory of Resource Chemistry of Ministry of Education, Shanghai Key Laboratory of Rare Earth Functional Materials, and Department of Chemistry, Shanghai Normal University, Shanghai 200234, P. R. China

[‡]Shanghai Synchrotron Radiation Facility, Shanghai Institute of Applied Physics, Chinese Academy of Sciences, Shanghai 201204, P. R. China

Supporting Information

ABSTRACT: A novel heterogeneous coordinatively unsaturated manganese monoxide-containing mesoporous carbon catalyst (C-MnO) is reported here. The catalysts exhibit high catalytic activity in wet oxidation of phenol (almost complete mineralization with an initial concentration of 50 mg/L at atmospheric pressure) and stability (reused 20 times without obvious activity loss or metal leaching), and they take more advantages than most developed heterogeneous Fenton catalysts. The one-pot surfactant self-assembly approach is used for the synthesis of the mesoporous C-MnO catalysts. Small-angle X-ray diffraction (XRD), N_2 sorption, and transmission electron microscopy results reveal that the catalysts have the ordered two-dimensional hexagonal mesostructure, large surface areas (530−552 m^2/g), uniform pore sizes (3.3−5.4 nm), and large pore volumes (0.34−0.44 cm^3/g); MnO nanoparticles (<12 nm) are well dispersed inside carbon mesopore systems with high crystallinity. The wide-angle XRD pattern reveals the presence of cubic rock salt structure MnO, and the Mn K-edge X-ray absorption fine structure spectra confirms the low chemical valence and the coordination unsaturated state of Mn. The high activity and stability of C-MnO catalysts might be related to the mesostructure, carbon pore wall, and, more importantly, the confined undercoordinative MnO nanoparticles.

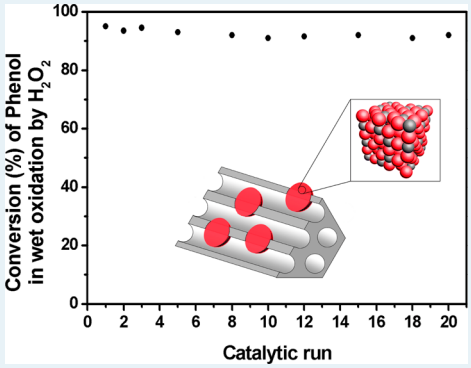

KEYWORDS: *manganese monoxide, carbon, mesostructure, coordinative unsaturation, confinement, oxidation*

1. INTRODUCTION

The coordinatively unsaturated metal sites that are confined by various ensembles such as hydrated ferryl ions, and iron-containing zeolites, show high reactivity and stability during oxidation.[1−4] Bao and co-workers found that the confinement of the coordinatively unsaturated metal sites with a low valence state is the key issue for the enhanced activity and stability during oxidation.[2] Both the interface-confined coordinatively unsaturated ferric sites and the Pt(111) supports are active in providing active oxygen species and highly efficient for carbon monoxide oxidation at low temperatures. The transition metal oxides, including Mn, Cu, etc., beyond Fe should also be studied because of their intrinsic oxidation ability.[5,6]

Catalytic wet oxidation using hydrogen peroxide as the oxidant is one of the most promising processes for removing persistent, toxic, and bioresistant phenolic compounds with low to medium-high total organic carbon (TOC) concentrations in wastewater, because this process is an efficient, inexpensive, and green chemical degradation.[7−9] Fenton-type catalysts are most frequently used. The major weakness of this homogeneous catalytic system is the involvement of a large amount of metallic salts that are presented in the effluents and require an additional separation step to separate metal-containing sludge, tight pH control, and the production of additional toxic wastes.[10,11] Therefore, the use of heterogeneous catalysts (such as Fe/ZSM-5[12]) is a promising alternative for which the principal goal is the development of efficient and stable solid catalysts for oxidation with minimal leaching of active species under the reaction conditions. The mesoporous support can play a major role in the adsorption of the organic compounds and subsequent reaction on the solid surface with active catalytic sites, resulting in remarkably enhanced performance.[13,14] A complete conversion of phenol in wet peroxide oxidation can be achieved in less than 15 min at 80 °C and 1 bar over iron-containing mesoporous silica MCM-41. However, the MCM-41 mesostructure would collapse upon long-term storage in the presence of moisture or by being stirred in an aqueous solution because of the thin wall thickness of silicates,[15,16] which can lead to metal deactivation. In addition, the leaching problem is severe, possibly because of the weak interaction of metal and support. Dissolution occurs in the reaction. In particular, less stable coordinatively unsaturated metal, e.g., Fe(II) and Cu(I), significantly leaches during the reaction, causing a loss of activity with time and generating a secondary metal ion problem.[17] For example, the amount of

Received: August 8, 2012
Published: October 18, 2012

   dx.doi.org/10.1021/cs300534y | *ACS Catal.* 2012, 2, 2577−2586

leached iron ions in zeolite and mesoporous silicas ranges from 10 to 90% depending on the synthesis route, the iron environment, and the concentration and strength of the acid sites presented.[18]

Carbon is a more convenient support for transition metal and oxides.[19] In this respect, a study of oxidation by ordered mesoporous carbon-based coordinatively unsaturated transition metal oxides is interesting and in demand. These coordinatively unsaturated oxides, which are confined both by element carbon and by a well-arranged nanopore matrix, would have great potential for oxidation. Recently, a self-assembly route has been reported for mesoporous carbons.[20,21] The self-assembling carbon mesostructures have uniform, tunable pore sizes and can be incorporated with SiO_2, carbides, metal oxides, and metal nanoparticles.[22−25] The Pd-containing catalysts derived thusly show good catalytic activity and stability in water-mediated coupling reactions,[13] but supported metal oxides with low chemical valence by mesoporous carbons have seldom been studied, possibly because they are easily oxidized to high chemical valence.[26,27]

In this work, we demonstrate a highly active and stable coordinatively unsaturated manganese monoxide-containing mesoporous carbon catalyst in the wet oxidation of phenol. Here metal-containing liquid crystals[28,29] and in situ reduction are used to synthesize mesoporous carbon embedded with MnO catalysts. The catalysts have the ordered two-dimensional (2D) hexagonal mesostructure, large surface areas, and uniform mespore sizes. Coordinatively unsaturated manganese monoxide with high crystallinity and <12 nm in size are introduced and well-dispersed inside carbon mesopores. The mesoporous carbon catalysts supported with MnO show a high phenol conversion activity over a wide pH range. Notably, the catalyst is very stable, showing negligible metal leaching and activity loss in successive catalytic runs. This behavior takes more advantage than most heterogeneous Fenton catalyst developed previously that suffers serious metal leaching.[30] Therefore, the excellent performance is attributed to the high activity of coordinatively unsaturated metal sites, the "sticky role" of amorphous carbon that stabilizes MnO nanoparticles and supports the structure without collapse during heating and stirring in solution, and the spatial confinement in the pores that facilitates the adsorption of phenol, accessibility to active sites, and mineralization of chemicals.

2. EXPERIMENTAL SECTION

2.1. Chemicals. Poly(ethylene oxide)-block-poly(propylene oxide)-block-poly(ethylene oxide) triblock copolymer F127 ($EO_{106}PO_{70}EO_{106}$, M_w = 12600), P123 ($EO_{20}PO_{70}EO_{20}$, M_w = 5800), and manganese(II) nitrate tetrahydrate [Mn-$(NO_3)_2{\cdot}4H_2O$] were obtained from Aldrich Chemical Co. Phenol (C_6H_5OH, 99.9 wt %), formaldehyde (HCHO, 37.0−40.0 wt %), sodium hydroxide (NaOH, 96 wt %), hydrogen chloride (HCl, 36.0−38.0 wt % solution in water), ethanol (C_2H_5OH, 99.7 wt %), acetone (C_3H_6O, 99.5 wt %), hydrogen peroxide (H_2O_2, 30 wt % solution in water), tetraethoxysilane (TEOS, 98 wt %), manganese(II) monoxide (MnO, 99.99 wt %), and manganese(II) chloride tetrahydrate ($MnCl_2{\cdot}4H_2O$, 99.0 wt %) were obtained from the Shanghai Chemical Co. All chemicals were used as received without any further purification. Water used in all syntheses was distilled and deionized.

2.2. Synthesis of Ordered Mesoporous C-MnO Nanocomposites. Mesoporous MnO-containing carbon nanocomposites were prepared from one-pot coassembly of weakly polymerized phenolic resins (the preparation procedure is described in the Supporting Information),[31] $Mn(NO_3)_2{\cdot}4H_2O$, and triblock copolymer F127. In a typical synthesis, 3.6 g of block copolymer F127 was dissolved in 24.0 g of ethanol while the mixture was being stirred at 40 °C to afford a clear solution. Then 1.11 g (4 mmol) of $Mn(NO_3)_2{\cdot}4H_2O$ was added to the clear solution while it was being stirred for 1 h. To it was added 15.0 g of a 20 wt % phenolic resin ethanolic solution while the mixture was being stirred for an additional 1 h. The mixture was transferred into multiple dishes. These dishes were then placed in a hood to evaporate ethanol at room temperature for 5−8 h and, subsequently, in an oven to thermopolymerize Bakelite at 100 °C for 24 h. The transparent films made thusly were scraped from the dishes, ground into fine powders, and placed in a quartz boat, and the boat was placed in a tubular oven. The powders were calcined at 600 °C in high-purity nitrogen (99.99%) for 6 h to remove the triblock copolymer templates, carbonize the matrix, and decompose and reduce the transition oxide. The ordered mesoporous products are denoted as C-MnO(x). The number in the sample name (x) represents the theoretical percent weight content of MnO in the composite from the ICP-AES analysis that was calcined at 600 °C. In a separate synthesis, $MnCl_2{\cdot}4H_2O$ was used to replace Mn-$(NO_3)_2{\cdot}4H_2O$. The final product is named C-MnO(x,Cl).

For the purpose of comparison, the powders made thusly were calcined at 600 °C in an oxygen-containing nitrogen atmosphere with a volume ratio of 1.5 or 3.0% O_2 (v/v). These catalysts are denoted C-MnO(x)-O1 and C-MnO(x)-O2, respectively, where x is exactly the same as the value in the C-MnO(x) sample described above for the sake of simplification. It should be noted that the MnO content changed in the composite with a different calcination atmosphere. Manganese oxide-containing mesoporous carbon and silica catalysts were also synthesized by impregnation, as described in the Supporting Information.[32,33]

2.3. Characterization. The X-ray diffraction (XRD) measurements were taken on a Rigaku Dmax-3C diffractometer using Cu Kα radiation. N_2 adsorption−desorption isotherms were measured at 77 K with a Micromeritics TristarII3020 analyzer. Before measurements, the samples were degassed in a vacuum at 100 °C for at least 6 h. The Brunauer−Emmett−Teller (BET) method was utilized to calculate the specific surface areas (S_{BET}). By using the Barrett−Joyner−Halenda (BJH) model, the pore volumes and pore size distributions were derived from the adsorption branches of isotherms. The micropore volumes (V_m) and micropore surface areas were calculated from the V−t plot method. Transmission electron microscopy (TEM) experiments were conducted on a JEM 2100 microscope operated at 200 kV. The samples for TEM measurements were suspended in ethanol and supported by a holey carbon film on a Cu grid. Energy dispersive X-ray spectroscopy (EDX) was performed on a Philips EDAX instrument. X-ray photoelectron spectroscopy (XPS) measurements were performed on a Perkin-Elmer PHI 5000CESCA system with a base pressure of 10^{-9} Torr. The energy positions of the peaks were calibrated by fixing the position of the C1s peak at 284.6 eV. Weight losses and the associated temperature were determined by thermogravimetry analysis with a Mettler Toledo TG/SDTA 851e apparatus. The metal ion concentrations were quantified using inductively coupled plasma-atomic emission spectroscopy (ICP-AES, VISTA-MPX). The X-ray absorption spectra data at the Mn K-edge were recorded

Table 1. Structural and Textural Properties for Mesoporous MnO-Containing Carbon Catalysts

catalyst	MnO content[a] (wt %)	a_0 (nm)	S_{BET} (m^2/g)	V_t (cm^3/g)	V_{micro} (cm^3/g)	D_p (nm)
C-MnO(5.4)	5.4	11.1	547	0.34	0.11	3.3
C-MnO(9.7)	9.7	11.5	552	0.43	0.13	4.7
C-MnO(17.8)	17.8	11.7	530	0.44	0.13	5.4
C-MnO(27.1)	27.1	*b*	332	0.31	0.04	*b*
C-MnO(17.8)-O1	18.4[c]	12.1	488	0.42	0.11	5.4
C-MnO(17.8)-O2	20.3[d]	12.0	518	0.47	0.11	5.8
C-MnO(17.8)-AE	17.8	11.5	374	0.34	0.05	5.3
Mn(im,Cl)-C(18)	19.2	11.3	284	0.22	0.02	<2
mesoporous carbon	0	11.4	888	0.68	0.22	4.7
Mn(im,Cl)-SiO_2(18)	17.1[d]	10.9	359	0.60	0.02	7.5
mesoporous SiO_2 SBA-15	0	11.1	779	1.00	0.06	8.8
C-MnO(17.8)-5	17.8	11.9	503	0.41	0.08	5.2

[a]Estimated from ICP-AES analysis. [b]Not detected. [c]This catalyst contains MnO and Mn_3O_4; the content of MnO is estimated from the total Mn content for the sake of simplification. [d]The content of Mn_3O_4, which is the major phase in this catalyst.

at room temperature in transmission mode using ion chambers at beamline BL14W1 of the Shanghai Synchrotron Radiation Facility. The station was operated with a Si(111) double-crystal monochromator. Energy calibrations were conducted using Mn foil for the Mn K-edge. Data processing was performed using ATHENA. All fits to the EXAFS data were performed using ARTEMIS.[34]

2.4. Wet Peroxidation of Phenol. To determine the catalytic activity of the samples, we selected the reported conditions for phenol degradation.[35−37] Catalytic oxidation was conducted in an ordinary pressure-stirred reactor. Before the reaction, all the catalysts were dried in the muffle furnace at 150 °C for 6 h. In a standard experiment, 0.1 g of Mn-containing solid catalyst was mixed with 50 mL of phenol (100 mg/L) and 0.15 mL of H_2O_2 (30 wt %) in a cylindrical water-jacketed glass cell. H_2O_2 was in excess. The mixture was stirred at 60 °C for different time intervals. The initial pH was adjusted to the required initial pH value by using HCl (0.1 mol/L) or NaOH (0.1 mol/L). After the reactions, the aliquot was hot filtrated and washed with 10 mL of ethanol with an ultrasonic device three times. The collected liquids (including the reaction product and product of desorption by ethanol) were analyzed on a high-performance liquid phase chromatograph (Agilent 1100) using a C18 reversed phase column with UV detection (UV 6000 diode array detector, Thermo Finnigan). The wavelength was set to 254 nm for phenol. Catalytic results are shown in terms of the absolute conversion of phenol, initial rate values (millimoles of reacted phenol per gram of catalyst per hour), calculated at the beginning of the reaction (15 min), or turnover frequency (TOF, millimoles per liter of reacted phenol per millimole per liter of MnO per hour) at 50% phenol degradation. Before and after the reaction, the total organic carbon (TOC) value was determined by a TOC analyzer (TOC-VCSH, Shimadzu). In some selected reactions, the reactor was hermetically sealed and connected to a gas buret to ensure a constant pressure (1 atm).[38] Carbon dioxide (CO_2) was analyzed using a gas chromatograph (Agilent 7890A) equipped with a Porapak Q column (1/4 in., 1 m) and a thermal conductivity detector (TCD) that was regularly sampled using a gas syringe. Carbon balance was then determined at different time intervals. The catalyst weight was determined for some selected reactions. At the end of the reaction, the catalyst was filtered and submitted to continuous solid−liquid extraction with ethanol using micro-Soxhlet equipment. Then the solvent was evaporated. The catalyst was weighed. It should be mentioned that the catalyst weight change is in the range of ±2%.

For the recycling study, the wet oxidation reaction was performed with phenol and H_2O_2, maintaining the same reaction conditions described above except using the recovered catalyst. Each time, after the completion of the reaction, the catalyst was recovered by hot filtration and then washed thoroughly with ethanol with an ultrasonic device. The recovered catalyst was dried under vacuum at 100 °C overnight, weighed, and reused in the next run. The solutions including reaction products and the elution solution were collected to determine the level of leaching of Mn after run 20. The reused catalyst is denoted C-MnO(*x*)-*y*, where *y* is the reaction time.

The adsorption of phenol was also studied by continuously shaking 50 mL of the aqueous mixture containing phenol and 0.1 g of C-MnO(17.8) in 100 mL flasks in a water bath shaker at 60 °C for 24 h under atmospheric pressure. The mixture was hot centrifuged and analyzed.

3. RESULTS

3.1. Structure of Coordinatively Unsaturated MnO-Containing Carbon Nanocomposites. Mesoporous MnO-containing carbon nanocomposites were synthesized by a combination of surfactant self-assembly using metal-containing liquid crystal and in situ reduction. The films made thusly are yellowish-brown and transparent without obvious macrophase separation. After being heated at 350−600 °C in a protecting atmosphere, the powders were uniform and became dark brown or black.

The Mn contents of the catalysts are estimated by ICP-AES (Table 1). Calculated levels of 5.4, 9.7, 17.8, and 27.1 wt % MnO iare present in composites C-MnO(5.4), -(9.7), -(17.8), and -(27.1), respectively. TG curves in air display a distinct weight loss together with two exothermal peaks for all studied carbon-based oxides corresponding to the combustion of carbon (Figure S1 of the Supporting Information). The MnO contents estimated from the molar equivalent of manganese in the ash components are 9.7 wt % for C-MnO(9.7) and 19.8 wt % for C-MnO(17.8), in agreement with the ICP-AES analysis. It should be noted that the final ash product after TG analysis is Mn_3O_4 instead of MnO. A parallel combustion test for C-MnO(17.8) was conducted in a muffle furnace at 600 °C in air. The solid was collected and proved to be Mn_3O_4 by the XRD pattern (Figure S2 of the Supporting Information).

dx.doi.org/10.1021/cs300534y | ACS Catal. 2012, 2, 2577−2586

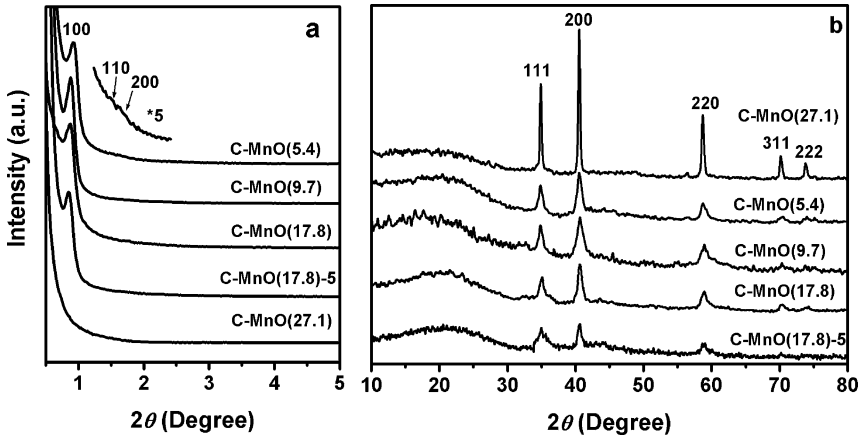

Figure 1. (a) Small-angle and (b) wide-angle XRD patterns for MnO-containing mesoporous carbon catalysts calcined at 600 °C under an inert atmosphere with different Mn loadings. The number in parentheses denotes the theoretical MnO mass content of the catalyst estimated by ICP-AES analysis. C-MnO(17.8)-5 represents a catalyst reused five times in the wet oxidation of phenol.

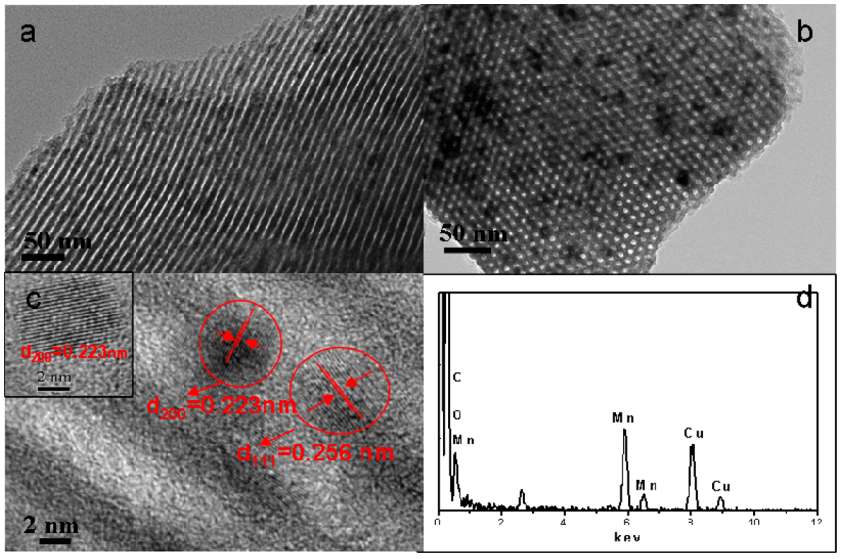

Figure 2. (a and b) TEM and (c) HRTEM images and (d) EDX pattern of C-MnO(17.8), viewed along the (a and c) [100] and (b) [001] directions. The inset in panel c is the HRTEM image.

The catalysts calcined at 600 °C under high-purity nitrogen with a MnO content of <20 wt % show the typical low-angle reflections characteristic of 2D hexagonal symmetry in space group *p6mm*, indicative of the ordered mesostructure (Figure 1a). The cell parameters are calculated to be ~11.0 nm, similar to that of pristine mesoporous carbon synthesized from F127 (11.1 nm).[33] The wide-angle XRD patterns (Figure 1b) exhibit the highly crystalline peaks that can be matched to the series of Bragg reflections corresponding to the pure cubic rock salt structure of MnO (*Fm*3*m*; a_0 = 4.445 nm). The particle sizes, estimated from the Scherrer formula, are 12.0 nm, regardless of the Mn content (5.4−17.8 wt %). However, the catalyst containing 27.1 wt % MnO does not possess the ordered mesostructure. The featured diffractions in the small-angle range disappear. At the same time, the wide-angle XRD gives a well-resolved pattern with narrow peaks, implying that the MnO species aggregate together. The estimated particle size is ~27.5 nm.

TEM images for C-MnO(17.8) show stripelike and hexagonally arranged pores, further confirming the 2D hexagonal ordered mesostructure (Figure 2a,b), and some dark dots highly dispersed inside the matrix. The EDX pattern (Figure 2d) reveals the presence of the Mn element. Therefore, the black dots in the TEM images should be MnO nanoparticles because its density is much higher than that of carbon. High-resolution TEM (HRTEM) images further reveal that the pore system of C-MnO(17.8) is composed of a large amount of nanoparticles and amorphous substance. The nanoparticles ~13 nm in size are well-dispersed and conglutinated by the amorphous substance in the whole framework (Figure 2c). It should be noted that nanoparticle sizes are smaller than $D_p + a_0$. That means one nanoparticle cannot penetrate two adjacent pore walls. In large areas, the *d* spacing of these nanocrystals is 0.256 and 0.223 nm, related to the (111) and (200) planes of MnO, respectively. These results are in good agreement with the size analysis from reflection broadening and phase identification in the XRD patterns. Careful analysis of many areas of this sample proves that no larger domains of MnO particles are located on the external surface of the carbon framework, indicating that MnO nanoparticles are selectively and spatially confined inside the carbon mesostructure.

dx.doi.org/10.1021/cs300534y | *ACS Catal.* 2012, 2, 2577−2586

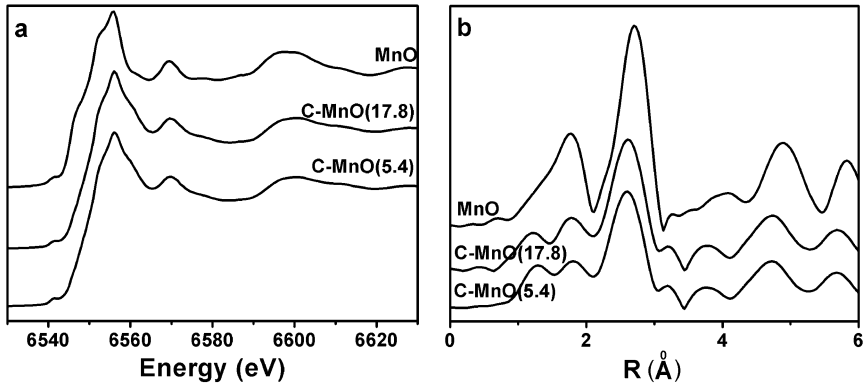

Figure 3. (a) Mn K-edge XANES spectra and (b) Fourier transform of Mn K-edge EXAFS spectra for C-MnO(5.4), C-MnO(17.8), and reference MnO.

Table 2. Fit Parameters of Mn K-Edge EXAFS Spectra for C-MnO(5.4), C-MnO(17.8), and Reference MnO

sample	shell	N^a	R^b	σ^2 ($\times 10^{-3}$ Å^2)^c	ΔE_0 (eV)^d
C-MnO(5.4)	Mn−C/O	1.5 ± 0.3	1.85 ± 0.01	10.4 ± 4.7	8.7 ± 1.5
	Mn−O	0.5 ± 0.1	2.26 ± 0.02	4.6 ± 1.9	−11.1 ± 1.7
	Mn−Mn	5.7 ± 0.5	3.11 ± 0.02	11.4 ± 1.1	−5.6 ± 2.2
C-MnO(17.8)	Mn−C/O	1.3 ± 0.2	1.78 ± 0.01	9.1 ± 4.1	8.1 ± 1.2
	Mn−O	0.6 ± 0.1	2.28 ± 0.02	6.1 ± 1.1	−14.7 ± 3.9
	Mn−Mn	7.9 ± 1.5	3.10 ± 0.02	15.0 ± 3.7	−5.5 ± 1.8
MnO	Mn−O	2.4 ± 0.5	2.21 ± 0.01	5.7 ± 3.9	4.6 ± 2.3
	Mn−Mn	11.5 ± 0.6	3.14 ± 0.01	12.3 ± 1.2	1.6 ± 1.1

^{a}Coordination number. ^{b}Distance between absorber and back-scatterer atoms. ^{c}Debye−Waller factor. ^{d}Inner potential correction.

The C-MnO(5.4) composite displays an XPS spectrum with only the C and O elements (Figure S3 of the Supporting Information). The surface and near-surface concentration of manganese is below or just at the detection limit. C-MnO(17.8) with a higher Mn content shows two very weak $Mn2p_{3/2}$ and $Mn2p_{1/2}$ peaks. These results indicate that the MnO nanoparticles are embedded in the carbon pore system. Similar results have been found in the immobilization of γ-Fe_2O_3 or cubic NiO in the carbon mesopores.[23,39] An undetectable signal is found via XPS analysis (a sampling volume from the surface to a depth of 1−5 nm), because of the embedding of metal in the carbon walls.[23,39]

The normalized XANES spectra at the Mn K-edge of the MnO-containing mesoporous carbon catalysts as well as the MnO reference are illustrated in Figure 3a. The catalysts exhibit well-defined, distinct XANES features. The small pre-edge peaks in XANES are attributed to the 1s → 3d transition. Both C-MnO(5.4) and C-MnO(17.8) samples show almost identical pre-edge features, similar to the MnO reference sample, indicating that the valence of manganese ion species in these samples is similar to that of MnO, regardless of the Mn content.[40,41] The Fourier transforms of the EXAFS data for the MnO reference show two strong peaks at 1.8 and 2.7 Å, which can be assigned to Mn−O coordination on the first shell with a coordination number (CN) of ∼2.4 and Mn−Mn coordination on the second shell with a CN of ∼11.5, respectively (Figure 3b and Table 2). Compared to the bulk crystalline MnO, both C-MnO(5.4) and C-MnO(17.8) show much smaller CNs for Mn−O and Mn−Mn bonds than bulk MnO. This is probably due to the nano effect of highly dispersive MnO species and unsaturated Mn−O bonds.[42,43] Interestingly, the Mn−O coordination splits into two peaks. The Mn−O bond at 2.3 Å shows a much lower CN of 0.5 for C-MnO(5.4) than the MnO reference, confirming the undercoordination. The other Mn−O bond at 1.8 Å is much shorter than the ordinary Mn−O bond. This result implies the structural distortion. Here we also could not exclude the doping of the carbon element in MnO during high-temperature carbonization because the backscattering factors of C and O are very close. This implies the interaction between element carbon and Mn.

All catalysts are found to have type IV N_2 sorption isotherms with distinct capillary condensation steps at relative pressures (p/p_0) of 0.4−0.65, which is typical for mesoporous solids with uniform pore sizes (Figure S4 of the Supporting Information). The pore size distribution curves for the mesoporous MnO-C composites calculated by the BJH method indeed show the narrow peaks centered at 3.3−5.4 nm, proving the ordered mesostructure and coincident with the XRD and TEM results. The H2-type hysteresis loop is observed for all catalysts, suggesting roughly cylindrical pores, and is analogous to the reported self-assembling mesoporous carbons.[44−46] The catalysts have large surface areas [530−552 m^2/g (Table 1)] and large pore volumes (0.34−0.44 cm^3/g). The *t* plot analysis reveals that the catalysts possess micropores (0.11−0.13 cm^3/g). By comparison, the pristine mesoporous carbon has a specific BET surface area of 888 m^2/g and a pore volume of 0.68 cm^3/g, including the micropore volume of 0.22 cm^3/g. The micropores in pore walls that originate from the release of small molecules during carbonization of resins contribute a large proportion of specific area.[33] If <3 nm amorphous inorganic nanoparticles are incorporated and homogeneously dispersed inside carbonaceous pore walls, the micropore volume of mesoporous carbon-based material is dramatically reduced to zero.[24,47] Accordingly, the materials possess a BET surface area as small as 350 m^2/g. Therefore, the decrease in BET surface area for these mesoporous MnO-C composites

dx.doi.org/10.1021/cs300534y | ACS Catal. 2012, 2, 2577−2586

upon comparison with that for the pristine mesoporous carbon is possibly due to the reduction in micropores inside carbonaceous pore walls that are immobilized with MnO nanoparticles. On the other hand, the involvement of MnO in the composite and its high density (~4.7 g/cm^3) should also be considered. This may lead to a reduction in the specific surface area for the composite, which is normally observed for the mesoporous nonsilica oxide materials.[48,49]

3.2. Catalytic Wet Peroxide Oxidation of Phenol. The main purpose of this work is to assess the influence of the preparation procedure on the catalytic activity of the Fenton reaction of mesoporous carbon-based coordinatively unsaturated manganese monoxide nanoparticles and to provide a reliable protocol for their preparation. To determine the catalytic activity of the samples, we selected the reported conditions for phenol degradation in the presence of the MnO-containing mesoporous carbon catalysts in which H_2O_2 is in excess.[50,51]

Using the sample C-MnO(17.8) as the catalyst, a 95% mineralization of phenol (initial concentration C_0 of 100 mg/L) during wet peroxide oxidation can be achieved at 60 °C, the natural pH value of 5.8 of the phenol solution, and atmospheric pressure with a reaction time of 6 h (Figure 4). It should be noted that the pH value increased to 7.3 once the catalyst was added into the solution because of the adsorption of phenol inside mesopores from water. The time conversion was obtained from different reaction batches with the same catalyst. The high activity is superior to most reported mesoporous heterogeneous catalysts. For example, Mn-containing MCM-41 exhibited a 95% conversion of phenol at pH 9 under a high pressure.[6] The Fe-containing SBA-15 catalyst could convert phenol only under either high pressure or UV−near-visible irradiation.[52] Even for a reaction with a fixed pH value ranging from 3 to 9, the high catalytic activity can be maintained. The oxidation can be conducted quite efficiently in the aqueous solution of phenol, and no acid needs to be added to decrease the pH to 2.0−3.0, which was needed by most heterogeneous Fe-containing Fenton-type catalysts.[36,53] This phenomenon may be related to the rapid adsorption of phenol, and the subsequent catalysis process inside mesopores of C-MnO. The initial reaction rate, at which the conditions are far from chemical equilibrium, is ~0.768 mmol h^{-1} g^{-1}.

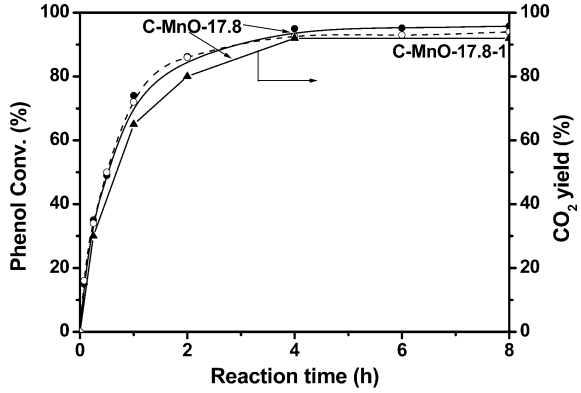

Figure 4. Time conversion plot for the conversion of phenol (● and ○) and yield of CO_2 (▲) in the wet oxidation of phenol (50 mL, 100 mg/L) by H_2O_2 (0.15 mL, 30 wt %) at 60 °C in the presence of fresh (solid lines and filled symbols) and used (dashed line and empty symbols) C-MnO(17.8).

Negligible oxidation intermediates are detected after the total reaction. The total organic carbon (TOC) conversion over C-MnO(17.8) was further tested, in which water is used to wash the catalyst instead of ethanol. Under limitation, the TOC value in the solution at the end of the reaction implies a total mineralization of phenol. Here we cannot completely exclude the formation of high-molecular weight substances or coke deposition during oxidation of phenol, which may not be eluted from the used catalyst. However, the yields of these substances are not high because of the catalyst weight change after reaction in the range of ±2%, which may be also caused by filtration and drying. The possible mechanism for the total oxidation of phenol can be illustrated as the final products are essentially CO_2 and H_2O through the formation of several intermediates.[54] Indeed, trace benzoquinone, hydroquinone, and catechol can be detected, when the reaction time is <2 h, but oxalic acid or acetic acid is not observed, as in the literature,[36] perhaps because of the extremely low concentration for those species. We further traced the formation of CO_2 during the reaction over C-MnO(17.8) (Figure 4). Carbon dioxide is generated through the degradation process at the very beginning, and its level increases with an increasing reaction time. The difference between the conversion and CO_2 yield in the middle reaction time may reflect the formation of oxidation intermediates. At the end of the reaction, CO_2 is detected as the only oxidative product. The total carbon mass balance can be obtained via the whole process (here we cannot completely exclude the formation of carbonaceous substances, because the final CO_2 concentration is slightly lower than expected). These phenomena imply that the partial oxidation takes place during the reaction and finally the oxidized intermediates can be completely converted.

Hot infiltration was adopted to detect the leaching of metal in the C-MnO(17.8) catalyst after reaction. Negligible Mn ions can be detected in solution. To further rule out the effect by Mn^{2+} ions, a reaction with the catalyst was stopped at 0.5 h, and 49% phenol conversion was obtained. Then the solid catalyst was taken out by hot infiltration. The liquid mixture was heated to 60 °C for further reaction. No more phenol conversion was detected. Therefore, a homogeneous oxidation by Mn^{2+} in solution can be excluded. This behavior shows that this new catalyst has great advantages versus Fe-based porous catalysts that undergo a remarkable metal leaching during the wet oxidation.[18] For example, solid Fe-containing porous catalyst suffers a 10−90% ion leaching, although the porous matrix plays a positive role in the enhancement of catalytic performance.[18]

Undetectable phenol was found in residue water after separation with solid mesoporous C-MnO catalysts, and only upon elution of the catalyst can phenol be detected, indicating the adsorption in pores. The adsorption isotherms of phenol belong to a type I curve, characteristic of monolayer Langmuir isotherms. The amount of adsorbed phenol dramatically increases at a lower final solution concentration, suggesting a high affinity between the dye molecule and the carbonaceous adsorbent surface,[55] and the adsorbed amount reaches a plateau at a higher equilibrium solution concentration, reflecting the saturated adsorption amount of 168 mg/g under these conditions (Figure 5). These observations are similar to those over pristine mesoporous carbon. After adsorption, ~155 mg/g of adsorbed organic substances can be released when C-MnO(17.8) and the adsorbates are shaken with ethanol at the same temperature with an ultrasonic device, reflecting that only

dx.doi.org/10.1021/cs300534y | ACS Catal. 2012, 2, 2577−2586

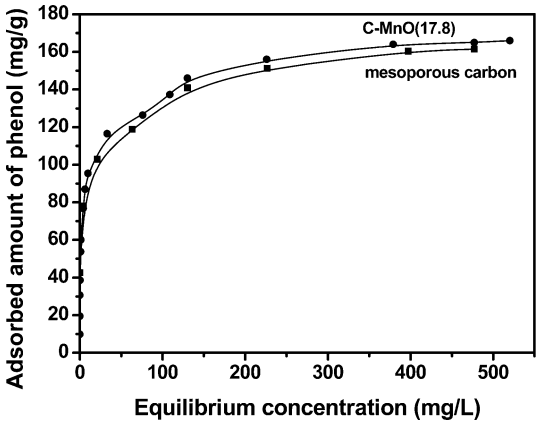

Figure 5. Adsorption isotherms for phenol on ordered mesoporous carbonaceous-based MnO catalyst C-MnO(17.8). For the sake of comparison, the adsorption on mesoporous carbon is also presented.

13 mg/g of phenol is residue inside pores after release even with a saturated adsorption. If the initial concentration for adsorption is 100 mg/L, more than 98% adsorbed phenol can be released. These results imply (1) the phenol can be fully adsorbed in the mesopores as the first step that is important for the subsequent catalytic reactions over active centers and (2) the adsorption of phenol in pores cannot be fully eluted by ethanol,[56] and accordingly, this part of phenol may also contribute to the total conversion of phenol during the wet oxidation over MnO-containing catalysts; however, the contribution is estimated to be small (<2% with an initial concentration of 100 mg/L).

This work also evaluates the efficiency of impregnated mesoporous catalysts. High-quality mesoporous carbon and silica are used as control material, as evidenced by the well-resolved small-angle XRD patterns (Figure 6a) and typical type

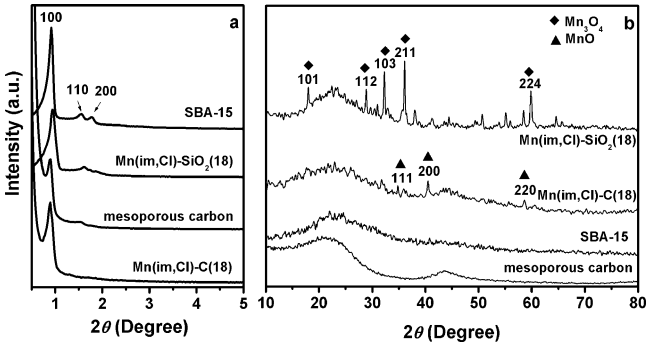

Figure 6. (a) Small-angle and (b) wide-angle XRD patterns for mesoporous carbon and silica SBA-15-supported MnO_x-containing catalysts. For comparison, the patterns for pristine mesoporous carbon and silica SBA-15 are also given.

IV N_2 sorption isotherms (Figure S6 of the Supporting Information). The BET surface area and pore volume are close to the values for mesoporous carbon FDU-15 and silica SBA-15 in the literature.[57,58] It should be noted that the Mn_3O_4 phase is involved in the final product in these catalysts using $Mn(NO_3)_2{\cdot}4H_2O$ as the initial Mn source regardless of the mesoporous carbon and silica carriers, even though a high purity of nitrogen is fed into the furnace during calcination (Figure S7 of the Supporting Information). This fact indicates the oxidation of MnO by an oxidant in the atmosphere probably originated from nitrate decomposition. Therefore, $MnCl_2{\cdot}4H_2O$ was used as the Mn source for impregnation. MnO supported on ordered mesoporous carbon can therefore be obtained with an estimated particle size of ~7.0 nm [from the Scherrer equation (Figure 6)]. However, pore blockage occurs. The BET surface area dramatically decreases from 888 to 284 m^2/g after impregnation, and the pore size decreases from 4.8 to 2.6 nm (Figure S6 of the Supporting Information). These observations indicate that some MnO nanoparticles are located inside mesoporous carbon pores while some are located at the orifice of pores. By comparison, the predominant phase of *I*41/*amd*(141) Mn_3O_4 is detected in the impregnated catalyst in the case of the silica SBA-15 support, implying the participation of surface active hydroxyl groups on silica in the oxidation of MnO. Some large particles (~26 nm) aggregate together (Figure 6), although the ordered mesostructure with a domain size of 7.5 nm can be retained. Upon consideration of the mass content and density (~4.8 g/mL) for Mn_3O_4, the decrease in surface area for Mn(im,Cl)-SiO_2(18) compared to that of pristine SBA-15 exists mainly because of the presence of large metal oxide crystals that do not contribute BET surface area.

After reaction, 56 and 21% phenol can be converted over Mn(im,Cl)-C(18) and Mn(im,Cl)-SiO_2(18), respectively, demonstrating MnO with nanoparticle sizes of 7.0 nm in Mn(im,Cl)-C(18) is more active during wet oxidation. However, the values are much lower than that over C-MnO(17.8). The possible reasons are that MnO active sites are accessible to adsorbed phenol molecules in large mesopores of C-MnO(17.8) while the orifice poisoning would occur over Mn(im,Cl)-C(18), and the coordination unsaturated MnO particles confined by carbon mesopores in the former provide more active oxygen species in the reaction. Leaching of Mn ions in Mn(im,Cl)-SiO_2(18) and Mn(im,Cl)-C(18) has been clearly detected by ~3.63 and ~8.75 mg/g, respectively. Homogeneous reactions due to manganese ions dissolved from the catalysts also contribute to the overall performance. These results are analogous to those for reported Fe-containing zeolite and mesoporous SBA-15 materials, a weak conversion of phenol at atmosphere pressure together with serious leaching.[59,60]

3.3. Reusability. After each reaction, the catalyst was hot filtered to inhibit the possible readsorption of leaching metal ions, eluted thoroughly by ethanol to eliminate surface-adsorbed substances, and subjected to the next run. The initial reaction rate for the second run (0.752 mmol h^{-1} g^{-1}) is similar with the refresh catalyst. The conversion almost retains a stable level in the following 20 runs (Figure 7). Therefore, the catalyst can be recovered. The reused C-MnO(17.8)-5 catalyst displays small-angle and wide-angle XRD patterns similar to that of the fresh one (Figure 1), characteristic of ordered mesostructure and cubic structure of MnO with an estimated particle size of 12 nm, indicating high stability. Finally, the reaction solutions after each run were mixed together to measure the Mn ion content. Less than 0.29 mg/g (~0.21%) determined leaching Mn ions demonstrates the stability of the oxide in the carbon framework.

4. DISCUSSION

The heterogeneous coordinatively unsaturated manganese monoxide-containing mesoporous carbon catalyst (C-MnO) shows high activity for wet oxidation of phenol and stability

dx.doi.org/10.1021/cs300534y | *ACS Catal.* 2012, 2, 2577−2586

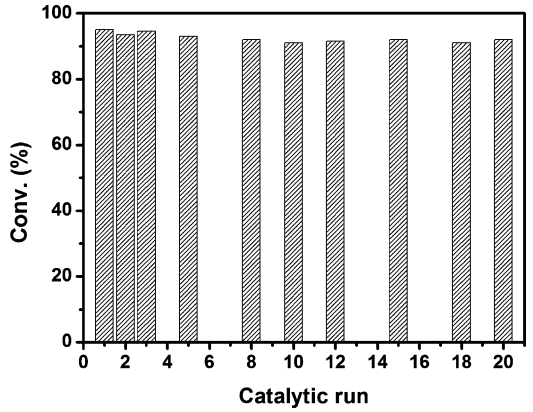

Figure 7. Catalytic performance of fresh and recovered C-MnO(17.8) catalyst in successive wet oxidation runs. After each run, the catalyst is recovered by hot centrifugation, washing with ethanol with an ultrasonic device and drying, and used in the successive runs.

with negligible metal leaching in reuse. Here three issues should be emphasized.

The first issue is the active sites of undercoordinative MnO with low chemical valence. The active oxygen species in C-MnO can attack substrates and leads to an enhancement of conversion. For comparison, the catalytic performance of C-MnO(17.8)-O1 and C-MnO(17.8)-O2 was also tested. These catalysts were prepared with 1.5 and 3.0% O_2 feeding in N_2. After carbonization, the total Mn contents are slightly increased, implying the slight loss of carbon during carbonization under an oxygen-containing atmosphere (Table 1). Both samples show the appearance of the oxidized phase of Mn_3O_4 (hausmannite structure, $I41/amd$) with high chemical valence, as evidenced by the XRD diffractions (Figure 8b). The

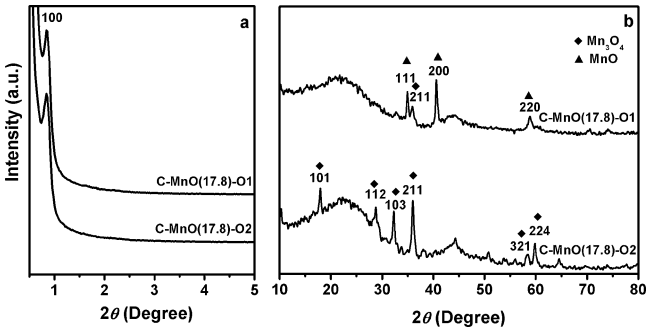

Figure 8. (a) Small-angle and (b) wide-angle XRD patterns for Mn-containing mesoporous carbon catalysts carbonized at 600 °C in an oxygen-containing atmosphere. O1 denotes a 1.5% O_2/N_2 mixture (v/v), and O2 denotes a 3.0% O_2/N_2 mixture (v/v).

particle sizes in C-MnO(17.8)-O1 and C-MnO(17.8)-O2 estimated from the broad diffraction peaks are ~13 nm. The aggregation of oxides is restricted. Because the samples are derived from the same as-made material as C-MnO(17.8) carbonized in high-purity nitrogen, these phenomena demonstrate that oxidation of MnO occurs in the presence of an oxidizing agent during calcination, and in accordance with the reports for the formation of Mn_3O_4 nanocrystals from MnO under controlled chemical oxidation.[26,61] The small-angle XRD patterns of C-MnO(17.8)-O1 and C-MnO(17.8)-O2 reflect the ordered 2D hexagonal mesostructure, indicating the stability of the mesostructure in an oxygen-containing atmosphere (Figure 8a). The confined oxidation of nanoparticles inside carbon mesopores is possibly responsible for the restriction of nanoparticle aggregation. N_2 sorption isotherms for both samples feature the mesopore structure with a uniform pore distribution (Figure S8 of the Supporting Information and Table 1), similar to C-MnO(17.8). A summary of the catalytic results given as turnover frequency values (TOF) measured at 50% of degraded phenol are presented in Table 3.[36] Compared

Table 3. Catalytic Results for Wet Oxidation of Phenol over Mn-Containing Catalysts[a]

catalyst	phase of MnO_x[b]	conversion (%)	TOF (h^{-1})[c]
C-MnO(17.8)	MnO	95	0.21
C-MnO(17.8)-O1	MnO/Mn_3O_4	52	0.017
C-MnO(17.8)-O2	Mn_3O_4	29	nd
Mn(im,Cl)-C(18)	MnO	56	0.016
Mn(im,Cl)-SiO_2(18)	Mn_3O_4	21	nd

[a]Oxidation reactions were conducted in air using 50 mL of phenol (100 mg/L), 0.15 mL of H_2O_2 (30 wt %), and 0.1 g of Mn-containing solid catalyst at 60 °C for 6 h. [b]Characterized by the XRD pattern. [c]TOF has been estimated by considering the number of phenol molecules degraded (millimoles per liter) per MnO molecule (millimoles per liter) in the required time to achieve 50% phenol degradation.[36]

to C-MnO(17.8), the two Mn_3O_4-containing catalysts both show lower phenol conversion after 6 h and a lower TOF value at 50% phenol degradation, especially over C-MnO(17.8)-O2 with a large amount of Mn_3O_4. The results further confirm the coordinatively unsaturated MnO serves as an active site for the wet oxidation of phenol under these conditions.

The second important issue is the confinement of MnO by a mesoporous carbon framework. The synthesis is based on self-assembly involving a metal-containing liquid crystal phase and in situ decomposition. Triblock copolymer self-assembly is induced by the presence of a nitrate salt with the homogeneous distribution of transition metal ions in the hydrophilic domains of the ordered mesophases.[28,29] The metal-containing liquid crystal phase can be formed only in a certain range.[28,29] Dag and co-workers found in general 0−8.0:1.0 transition metal:-EO-containing surfactant molar ratios.[28,29] Therefore, the Mn content is limited in the composite. Upon consideration of the interaction between triblock copolymer and phenolic resins, the ordered mesostrucure can be fixed with 0−16.0:1.0:65.0 Mn^{2+}:F127:phenol molar ratios. An overly high content in the composite catalyst, for example, 27.4% MnO, would lead to a disturbance of the ordered mesostructure. Without the confinement of the pore structure, large crystals are formed. This catalyst shows a low level (20%) of phenol conversion.

During high-temperature treatment, the clustering metal oxide particles would grow and become embedded within the carbon mesopores, rather than remaining dispersed on the external surfaces of the carbons. These phenomena suggest strong interactions of the MnO species with the carbon framework. Phenolic resin is used as a carbon source that can interact with and surround the liquid crystal phase to form an infinite "soft" polymeric framework. The transition metal species can further serve as the resin pyrolysis catalysts. Carbon deposits on the catalyst. The soft polymer framework is fixed to relatively "rigid" carbon, which can confine the growth of clustering oxide to some extent. The released reductive small molecules such as CO, CH_4, etc., can simultaneously inhibit the

dx.doi.org/10.1021/cs300534y | ACS Catal. 2012, 2, 2577−2586

oxidation of manganese species to high chemical valence during heat treatment in an inert atmosphere. Carbon may be doped into the MnO lattice as evidenced by the possible Mn−C bonds in the EXAFS analysis. Carbon can indeed modify the MnO surface energy through the interactions between them, which can result in the expression of surfaces with different structures. The exposure of these facets that can reduce the surface energy may also supply the coordination Mn−O bonds with high energy. The development of specific facets has been correlated with the surprising activity of transition metal oxides.[62,63] Under these conditions, the ∼12 nm under-coordinative MnO clusters confined by the carbon framework are formed. The MnO acts as the active center, which can provide active oxygen species, possibly similar to interface-confined coordinatively unsaturated ferric sites.[2]

It should be mentioned that the confined MnO particles in the framework would certainly not satisfy a complete atom efficiency. The TOF value is low, compared to those of Fe-containing and Au-contaning catalysts.[12,36,53] Partial MnO particles are exposed and accessible to chemicals and contribute to adsorption and reaction processes; in addition, partial MnO clusters are embedded inside walls that actually stabilize the catalyst in solution reactions. Similar results have also been reported in an active catalyst of the mesoporous SiO_2−TiO_2 composite in which anatase nanocrystals are embedded inside the silica framework.[64]

Lastly, the spatial confinement in the pores should also be addressed. Mesoporous C-MnO catalysts favor the adsorption of the organic compound inside the carbon mesopores, resulting in an increase in the effective organic concentration near the active site. Organic substrates and media, if any, can therefore be completely oxidized.

5. CONCLUSIONS

In this study, we have addressed a new ordered mesoporous coordinatively unsaturated MnO-containing carbon catalyst suitable for remediation of a trivial organic compound from contaminated water through a Fenton-like reaction with H_2O_2. The catalyst possesses a nanocomposite structure with coordinatively unsaturated manganese monoxide with high crystallinity and sizes of <12 nm immobilizing in the ordered mesoporous carbon mesopores, uniform pore sizes, large surface areas, and large pore volumes. The coordinatively unsaturated MnO sites are highly active for phenol oxidation. Amorphous carbon plays a sticky role for MnO nanoparticles for enhancing stability. The large mesopores favor mass transportation, and spatial confinement of reaction mixtures in the pores facilitates the accessibility to oxide active centers. These features endow the catalyst with a high phenol mineralization activity over a wide pH range (3−9), complete elimination of low-concentration phenol, good stability in the reaction with negligible leaching, and loss of activity after 20 runs, taking advantage more than most reported active Fenton-like heterogeneous catalysts. We believe that the mesoporous MnO-C catalyst can be an alternative choice for the most frequently used Fe-based Fenton catalysts, which have serious problems in terms of metal leaching.

■ ASSOCIATED CONTENT

Supporting Information

Preparation of soluble phenolic resins and impregnated mesoporous catalysts; TG/DTA curves, XPS spectra, N_2 adsorption−desorption isotherms, pore size distribution curves, and t plot analysis of MnO-containing carbon nanocomposites with different Mn contents; wide-angle XRD pattern, N_2 adsorption−desorption isotherms, pore size distribution curves, and t plot analysis of MnO-containing mesoporous carbon catalyst C-MnO(17.8) (fresh, after the adsorption−elution cycle, and after five reaction cylces); wide-angle XRD pattern, N_2 adsorption−desorption isotherms, and pore size distribution curves of pristine mesoporous supports (carbon and silica SBA-15) and impregnated MnO_x-containing catalysts; and N_2 adsorption−desorption isotherms and pore size distribution curves of Mn-containing mesoporous carbon catalysts calcined at 600 °C in an oxygen-containing atmosphere. This material is available free of charge via the Internet at http://pubs.acs.org.

■ AUTHOR INFORMATION

Corresponding Author

*Telephone: 86-21-6432-2516. Fax: 86-21-6432-2511. E-mail: ywan@shnu.edu.cn.

Notes

The authors declare no competing financial interest.

■ ACKNOWLEDGMENTS

This work was supported by the National Science Foundation of China (21073122 and 21173149), State Key Basic Research Program of PRC (2013CB934100), Shanghai Sci. & Tech. and Edu. Committee (10XD1403300, 11JC1409200, and S30406), and the Fok Ying Tung Education Fund (121013).

■ REFERENCES

(1) Fajerwerg, K.; Debellefontaine, H. *Appl. Catal., B* **1996**, *10*, L229.
(2) Fu, Q.; Li, W. X.; Yao, Y. X.; Liu, H. Y.; Su, H. Y.; Ma, D.; Gu, X. K.; Chen, L. M.; Wang, Z.; Zhang, H.; Wang, B.; Bao, X. H. *Science* **2010**, *328*, 1141.
(3) Guo, S.; Pan, X.; Yu, L.; Bao, X. *Mater. Lett.* **2011**, *65*, 1522.
(4) Zhang, H.; Pan, X.; Liu, J.; Qian, W.; Wei, F.; Huang, Y.; Bao, X. *ChemSusChem* **2010**, *4*, 975.
(5) Ben Achma, R.; Ghorbel, A.; Dafinov, A.; Medina, F. *Appl. Catal., A* **2008**, *349*, 20.
(6) Chaliha, S.; Bhattacharyya, K. G. *Ind. Eng. Chem. Res.* **2008**, *47*, 1370.
(7) Plant, L.; Jeff, M. *Chem. Eng. Environ. Eng.* **1994**, *101*, 16.
(8) Guo, J.; Al-Dahhan, M. *Ind. Eng. Chem. Res.* **2003**, *42*, 2450.
(9) Zazo, J. A.; Casas, J. A.; Mohedano, A. F.; Rodriguez, J. J. *Appl. Catal., B* **2006**, *65*, 261.
(10) Barrault, J.; Tatibouet, J. M.; Papayannakos, N. *C. R. Acad. Sci., Ser. II* **2000**, *3*, 777.
(11) Navalon, S.; Alvaro, M.; Garcia, H. *Appl. Catal., B* **2010**, *99*, 1.
(12) Kuznetsova, E. V.; Savinov, E. N.; Vostrikova, L. A.; Parmon, V. N. *Appl. Catal., B* **2004**, *51*, 165.
(13) Wan, Y.; Wang, H.; Zhao, Q.; Klingstedt, M.; Terasaki, O.; Zhao, D. *J. Am. Chem. Soc.* **2009**, *131*, 4541.
(14) Martinez, F.; Calleja, G.; Melero, J. A.; Molina, R. *Appl. Catal., B* **2007**, *70*, 452.
(15) Wan, Y.; Zhao, D. *Chem. Rev.* **2007**, *107*, 2821.
(16) Armengol, E.; Corma, A.; Fornés, V.; García, H.; Primo, J. *Appl. Catal., A* **1999**, *181*, 305.
(17) Valkaj, K. M.; Katovic, A.; Zrncevic, S. *J. Hazard. Mater.* **2007**, *144*, 663.
(18) Ovejero, G.; Sotelo, J. L.; Martínez, F.; Melero, J. A.; Gordo, L. *Ind. Eng. Chem. Res.* **2001**, *40*, 3921.
(19) Wan, Y.; Shi, Y. F.; Zhao, D. Y. *Chem. Mater.* **2008**, *20*, 932.
(20) Liang, C.; Hong, K.; Guiochon, G. A.; Mays, J. W.; Dai, S. *Angew. Chem., Int. Ed.* **2004**, *43*, 5785.
(21) Liang, C. D.; Dai, S. *J. Am. Chem. Soc.* **2006**, *128*, 5316.
(22) Yu, T.; Deng, Y.; Wang, L.; Liu, R.; Zhang, L.; Tu, B.; Zhao, D. *Adv. Mater.* **2007**, *19*, 2301.

(23) Wang, W.; Wang, H.-Y.; Wei, W.; Xiao, Z.-G.; Wan, Y. *Chem.—Eur. J.* **2011**, *17*, 13461.
(24) Liu, R.; Shi, Y.; Wan, Y.; Meng, Y.; Zhang, F.; Gu, D.; Chen, Z.; Tu, B.; Zhao, D. *J. Am. Chem. Soc.* **2006**, *128*, 11652.
(25) Gorka, J.; Jaroniec, M. *J. Phys. Chem. C* **2008**, *112*, 11657.
(26) Yin, M.; O'Brien, S. *J. Am. Chem. Soc.* **2003**, *125*, 10180.
(27) Si, H.; Wang, H.; Shen, H.; Zhou, C.; Li, S.; Lou, S.; Xu, W.; Du, Z.; Li, L. S. *CrystEngComm* **2009**, *11*, 1128.
(28) Çelik, Ö.; Dag, Ö. *Angew. Chem.* **2001**, *113*, 3915.
(29) Demirors, A. F.; Eser, B. E.; Dag, O. *Langmuir* **2005**, *21*, 4156.
(30) Hartmann, M.; Kullmann, S.; Keller, H. *J. Mater. Chem.* **2010**, *20*, 9002.
(31) Meng, Y.; Gu, D.; Zhang, F.; Shi, Y.; Yang, H.; Li, Z.; Yu, C.; Tu, B.; Zhao, D. *Angew. Chem., Int. Ed.* **2005**, *44*, 7053.
(32) Zhao, D.; Feng, J.; Huo, Q.; Melosh, N.; Fredrickson, G. H.; Chmelka, B. F.; Stucky, G. D. *Science* **1998**, *279*, 548.
(33) Meng, Y.; Gu, D.; Zhang, F.; Shi, Y.; Cheng, L.; Feng, D.; Wu, Z.; Chen, Z.; Wan, Y.; Stein, A.; Zhao, D. *Chem. Mater.* **2006**, *18*, 4447.
(34) Ravel, B.; Newville, M. *J. Synchrotron Radiat.* **2005**, *12*, 537.
(35) Quintanilla, A.; García-Rodríguez, S.; Domínguez, C. M.; Blasco, S.; Casas, J. A.; Rodriguez, J. J. *Appl. Catal., B* **2012**, *111−112*, 81.
(36) Martin, R.; Navalon, S.; Delgado, J. J.; Calvino, J. J.; Alvaro, M.; Garcia, H. *Chem.—Eur. J.* **2011**, *17*, 9494.
(37) Santos, A.; Yustos, P.; Rodriguez, S.; Simon, E.; Romero, A. *Ind. Eng. Chem. Res.* **2010**, *49*, 5583.
(38) Jiang, Y.; Pétrier, C.; David Waite, T. *Ultrason. Sonochem.* **2002**, *9*, 317.
(39) Lu, A.-H.; Nitz, J.-J.; Comotti, M.; Weidenthaler, C.; Schlichte, K.; Lehmann, C. W.; Terasaki, O.; Schuth, F. *J. Am. Chem. Soc.* **2010**, *132*, 14152.
(40) Fandeur, D.; Juillot, F.; Morin, G.; Olivi, L.; Cognigni, A.; Webb, S. M.; Ambrosi, J.-P.; Fritsch, E.; Guyot, F.; Brown, G. E., Jr. *Environ. Sci. Technol.* **2009**, *43*, 7384.
(41) Ribeiro, M. C.; Jacobs, G.; Pendyala, R.; Davis, B. H.; Cronauer, D. C.; Kropf, A. J.; Marshall, C. L. *J. Phys. Chem. C* **2011**, *115*, 4783.
(42) Kou, Y.; Zhang, B.; Niu, J.-z.; Li, S.-b.; Wang, H.-l.; Tanaka, T.; Yoshida, S. *J. Catal.* **1998**, *173*, 399.
(43) Tang, Q.; Huang, X.; Chen, Y.; Liu, T.; Yang, Y. *J. Mol. Catal. A: Chem.* **2009**, *301*, 24.
(44) Thommes, M.; Smarsly, B.; Groenewolt, M.; Ravikovitch, P. I.; Neimark, A. V. *Langmuir* **2006**, *22*, 756.
(45) Kleitz, F.; Czuryszkiewicz, T.; Solovyov, L. A.; Lindén, M. *Chem. Mater.* **2006**, *18*, 5070.
(46) Groen, J. C.; Peffer, L. A. A.; Pérez-Ramırez, J. *Microporous Mesoporous Mater.* **2003**, *60*, 1.
(47) Wang, W.; Zhuang, X.; Zhao, Q.; Wan, Y. *J. Mater. Chem.* **2012**, *22*, 15874.
(48) Thimsen, E.; Le Formal, F.; Grätzel, M.; Warren, S. C. *Nano Lett.* **2011**, *11*, 35.
(49) Lewicka, Z.; Benedetto, A.; Benoit, D.; Yu, W.; Fortner, J.; Colvin, V. *J. Nanopart. Res.* **2011**, *13*, 3607.
(50) Sun, H.; Tian, H.; Hardjono, Y.; Buckley, C. E.; Wang, S. *Catal. Today* **2012**, *186*, 63.
(51) Bayat, M.; Sohrabi, M.; Royaee, S. J. *J. Ind. Eng. Chem.* **2012**, *18*, 957.
(52) Martínez, F.; Calleja, G.; Melero, J. A.; Molina, R. *Appl. Catal., B* **2007**, *70*, 452.
(53) Navalon, S.; de Miguel, M.; Martin, R.; Alvaro, M.; Garcia, H. *J. Am. Chem. Soc.* **2011**, *133*, 2218.
(54) Fortuny, A.; Ferrer, C.; Bengoa, C.; Font, J.; Fabregat, A. *Catal. Today* **1995**, *24*, 79.
(55) Vinu, A.; Miyahara, M.; Ariga, K. *J. Phys. Chem. B* **2005**, *109*, 6436.
(56) Zhuang, X.; Wan, Y.; Feng, C.; Shen, Y.; Zhao, D. *Chem. Mater.* **2009**, *21*, 706.
(57) Meng, Y.; Gu, D.; Zhang, F.; Shi, Y.; Yang, H.; Li, Z.; Yu, C.; Tu, B.; Zhao, D. *Angew. Chem.* **2005**, *117*, 7215.
(58) Zhao, D.; Sun, J.; Li, Q.; Stucky, G. D. *Chem. Mater.* **2000**, *12*, 275.
(59) Gokulakrishnan, N.; Pandurangan, A.; Sinha, P. K. *Ind. Eng. Chem. Res.* **2009**, *48*, 1556.
(60) Melero, J. A.; Martínez, F.; Botas, J. A.; Molina, R.; Pariente, M. I. *Water Res.* **2009**, *43*, 4010.
(61) Hyeon, T.; Lee, S. S.; Park, J.; Chung, Y.; Na, H. B. *J. Am. Chem. Soc.* **2001**, *123*, 12798.
(62) Yang, H. G.; Sun, C. H.; Qiao, S. Z.; Zou, J.; Liu, G.; Smith, S. C.; Cheng, H. M.; Lu, G. Q. *Nature* **2008**, *453*, 638.
(63) Pan, J.; Liu, G.; Lu, G. Q.; Cheng, H.-M. *Angew. Chem., Int. Ed.* **2011**, *50*, 2133.
(64) Dong, W. Y.; Sun, Y. J.; Lee, C. W.; Hua, W. M.; Lu, X. C.; Shi, Y. F.; Zhang, S. C.; Chen, J. M.; Zhao, D. Y. *J. Am. Chem. Soc.* **2007**, *129*, 13894.